Design of Single-Atom Co−N_5 Catalytic Site: A Robust Electrocatalyst for CO_2 Reduction with Nearly 100% CO Selectivity and Remarkable Stability

Yuan Pan,[†,Δ] Rui Lin,[†,Δ] Yinjuan Chen,[†,§,Δ] Shoujie Liu,[†,⊥] Wei Zhu,[†] Xing Cao,[†] Wenxing Chen,[†] Konglin Wu,[†,⊥] Weng-Chon Cheong,[†] Yu Wang,[†] Lirong Zheng,[‡] Jun Luo,[//] Yan Lin,[§] Yunqi Liu,[§] Chenguang Liu,[§] Jun Li,[†] Qi Lu,[¶] Xin Chen,[#] Dingsheng Wang,[†] Qing Peng,[†] Chen Chen,*[,†] and Yadong Li[††]

Department of Chemistry, Tsinghua University, Beijing 100084, China

[§]State Key Laboratory of Heavy Oil Processing, China University of Petroleum (East China), Qingdao 266580, China

[⊥]College of Chemistry and Materials Science, Anhui Normal University, Wuhu 241000, China

[‡]Beijing Synchrotron Radiation Facility, Chinese Academy of Sciences, Beijing 100049, China

[//] Center for Electron Microscopy, Tianjin University of Technology, Tianjin 300384, China

[¶]Department of Chemical Engineering, Tsinghua University, Beijing 100084, China

[#]Department of Chemistry, University of Science and Technology Beijing, Beijing 100083, China

*S Supporting Information

ABSTRACT: We develop an N-coordination strategy to design a robust CO_2 reduction reaction (CO_2RR) electrocatalyst with atomically dispersed Co−N_5 site anchored on polymer-derived hollow N-doped porous carbon spheres. Our catalyst exhibits high selectivity for CO_2RR with CO Faradaic efficiency (FE_{CO}) above 90% over a wide potential range from −0.57 to −0.88 V (the FE_{CO} exceeded 99% at −0.73 and −0.79 V). The CO current density and FE_{CO} remained nearly unchanged after electrolyzing 10 h, revealing remarkable stability. Experi-ments and density functional theory calculations demon- strate single-atom Co−N_5 site is the dominating active center simultaneously for CO_2 activation, the rapid formation of key intermediate COOH* as well as the desorption of CO.

Electrocatalytic CO_2 reduction reaction (CO_2RR) is an important process for CO_2 conversion, and it could help tackle the global warming problem, resulting from excessive consumption of fossil fuels to some extent.[1,2] However, the existence of competitive process, namely hydrogen evolution reaction (HER), and the high overpotential in CO_2RR decrease the selectivity of product and conversion efficiency. A series of electrocatalysts including metals and molecular complexes, etc.[3−20] have been explored to improve the CO_2 reduction activity. Among them, due to the distinct molecular structure and tunable atomic structure, metal porphyrins and phthalo-cyanines were considered as optimal models to explore catalytic mechanism and optimize the catalytic performance.[21,22] Recently, N-doped carbon material anchored metal single CO_2RR.[26,27] Despite extensive efforts by researchers, the development of robust electrocatalysts to boost the catalytic performance and the exploration of active center for CO_2RR are still challenging.

Herein, we report a highly active and selective catalyst with atomically dispersed Co sites anchored on polymer-derived hollow N-doped porous carbon spheres (HNPCSs) with large surface area (568 $m^2 \cdot g^{-1}$), abundant coordination N sites and high electrical conductivity. Electrochemical measurements indicate that the Co−N_5/HNPCSs catalyst exhibits excellent performance for CO_2RR with CO Faradaic efficiency (FE_{CO}) of 99.2% and 99.4% at −0.73 and −0.79 V, which is equivalent to a 15.5-fold enhancement of cobalt phthalocyanine (CoPc) inactivity. This catalyst also exhibits high FE_{CO} (>90%) over a wide potential range

from −0.57 to −0.88 V. Combining experiments and density functional theory (DFT) calculations, we deduce single-atom Co−N_5 site is the dominating active center simultaneously for CO_2 activation and the rapid formation of key reaction intermediate COOH* as well as the desorption of CO.

Figure 1a shows the synthesis procedures. We synthesize core@shell SiO_2@melamine-resorcinol-formaldehyde polymer spheres (MRFPSs) using a modified Stober method[28] (Figure S1a). Then, SiO_2@N-doped porous carbon spheres are obtained by pyrolysis of SiO_2@MRFPSs at 700 °C under Ar (Figure S1b). After etching the silica core with HF, the HNPCSs were obtained (Figure S1c−g). Finally, the Co−N_5/ HNPCSs catalyst is prepared through constructing coordina-tion interaction between Co and N. A uniform hollow spherical structure can be observed (Figure 1b,c) from scanning electron microscopy (SEM) and transmission electron microscopy (TEM). These morphologies inherite the structure of HNPCSs, and no CoPc aggregates are observed, suggesting that CoPc are anchored on the HNPCSs uniformly. High-angle annular dark-field scanning transmission electron microscopy (HAADF-STEM) and energy-dispersive X-ray spectroscopy (EDS) images reveal that C, N and Co elements are homogeneously distributed over the entire HNPCSs (Figure 1d). The Co content (determined by inductively coupled plasma optical emission spectrometry) is about 3.54 wt % (Table S1). From aberration-corrected HAADF-STEM, high-density bright dots (highlighted by yellow circles) are observed (Figure 1e,f), which is corresponding to single Co atoms. The Raman spectrum (Figure S2) suggests the Co−N_5/HNPCSs catalyst only exhibits the vibrational peaks of HNPCSs, indicating the strong electronic interactions between CoPc and HNPCSs.

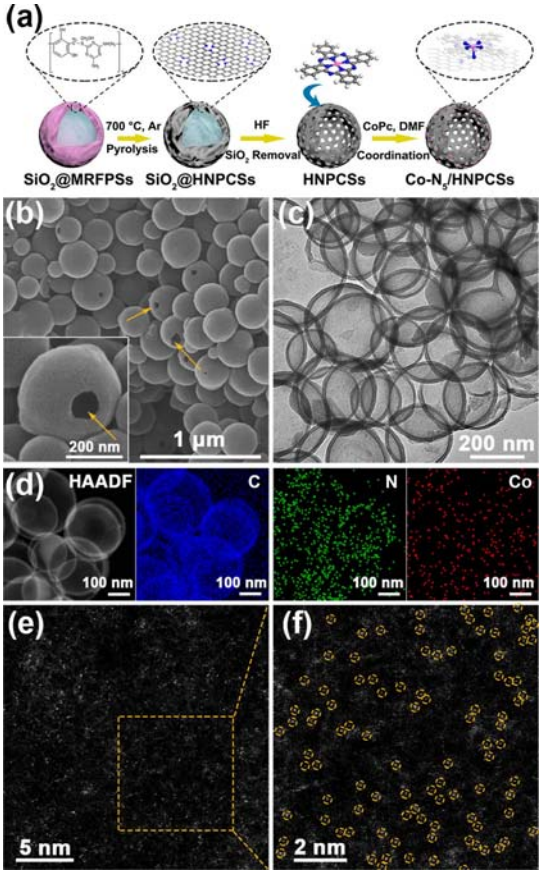

Figure 1. (a) Schematic illustration, (b) SEM, (c) TEM, (d) HAADF- STEM and EDS images, C (blue), N (green) and Co (red). (e, f) AC HAADF-STEM and magnified images.

The X-ray diffraction (XRD) pattern only displays a broad peak at 2θ = 22.8°, corresponding to the (002) plane of HNPCSs. No diffraction peak of CoPc is observed, indicating that CoPc is anchored on the HNPCSs with high dispersity (Figure S3). X-ray photoelectron spectroscopy (XPS) reveals the presence of C, N and Co elements (Figure S4a). The binding energy (BE) of the Co $2p_{3/2}$ peak located at 780.6 eV, corresponding to the Co−N species (Figure S4b). The BE of Co 2p is higher than that Co^0 (778.1 eV) and Co^{2+} (779.2 eV), but lower than that Co^{3+} (781 eV) (Figure S4d), suggesting the valence state of Co is between +2 and +3. Three types of N atoms including graphitic (401.3 eV), pyrrolic (400.2 eV) and pyridinic (398.8 eV) can be distinguished (Figure S4c). The pyrrolic-N species served as anchor for stabilizing the single atom Co site because of the existence of the strong coordination affinity, as confirmed by DFT (Figure S25). The Auger spectroscopy (Figure S4e,f) of Co−N_5/HNPCSs has a some shift about 6 eV to the right compared with CoPc, which indicates that the valence of Co atom in Co−N_5/HNPCSs is higher than that of CoPc, demonstrating the existence of coordination interaction.

The electronic structure and coordination environment are examined by X-ray absorption near-edge structure (XANES) and extended X-ray absorption fine structure (EXAFS). The absorption edge position of Co−N_5/HNPCSs is located between that of CoO and Co_3O_4, suggesting single Co atom carries positive charge and the valence state of Co is between +2 and +3 (Figure 2a). The Co K-edge exhibits a similar near-edge structure to that of CoPc but the curve has a minor shift to the right, which indicates that the valence of Co atom in Co−N_5/HNPCSs is slightly higher than that of CoPc.

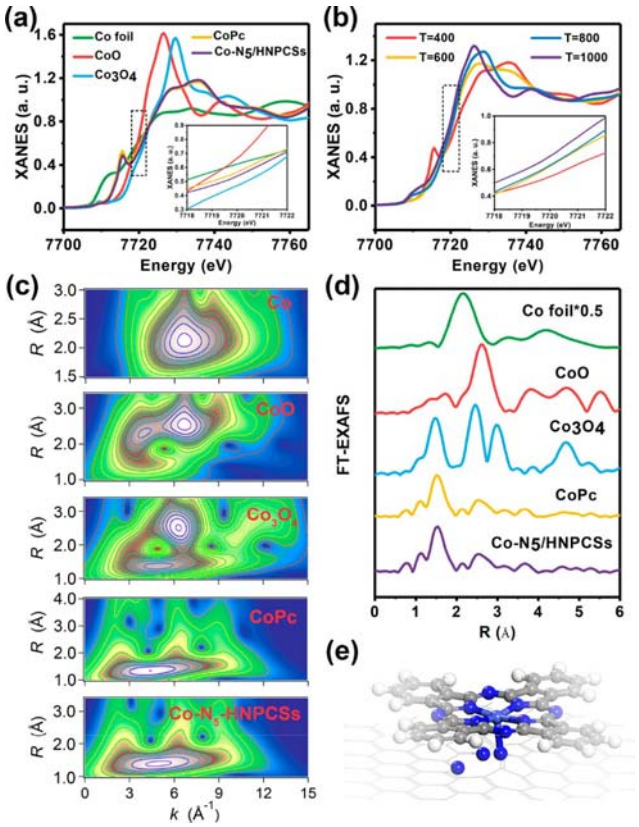

Figure 2. XANES spectra at the Co K-edge of (a) Co foil, CoO, Co3O4 and Co−N5/HNPCSs, (b) Co−N5/HNPCSs-T (inset is the magnified image), (c) WT, (d) FT at R space, (e) schematic model,Co (wathet), N (blue), C (gray) and H (white).

The Fourier-transformed (FT) k^3-weighted EXAFS spectra (Figure 2d) displays one main peak at 1.5 Å, corresponding to the Co− N first coordination shell, and no Co−Co coordination peak at Å can be detected. The wavelet transform (WT) plot (Figure 2c) of Co−N_5/HNPCSs shows the WT maximum at 5$Å^{-1}$, corresponding to the Co−N bonding by comparing with Co foil, CoO, Co_3O_4 and CoPc. No intensity maximum corresponded to Co−Co can be observed. Compared with CoPc, the slight shift of WT maximum may be due to the existence of coordination interaction between CoPc and HNPCSs. The quantitative coordination configuration of Co atom can be obtained by EXAFS fitting (Figure S5, Table S2). The Co−N coordination number is 5. These results further indicate that the existence of coordination between single Co atom in CoPc and N atom in HNPCSs. Therefore, the Co atomic structure model can be described (Figure 2e, the Co atom is coordinated by five N atoms).

The CO_2 electrolysis is measured by linear sweep voltammetry (LSV) in a CO_2-saturated 0.2 M $NaHCO_3$ solution (Figure 3a). The Co−N_5/HNPCSs shows 15.5-fold higher current densities (6.2 mA·cm^{-2}, normalized by the geometrical surface area) relative to pure CoPc (0.4 mA·cm^{-2}) at the potential of −0.73 V vs RHE. The FE_{CO} reaches 99.2% and 99.4% over Co−N_5/HNPCSs catalyst at −0.73 and −0.79 V vs RHE respectively, which is significantly higher than CoPc at the same potential (Figure 3b). Such high FE_{CO} has seldom been reported up to now (Table S3).

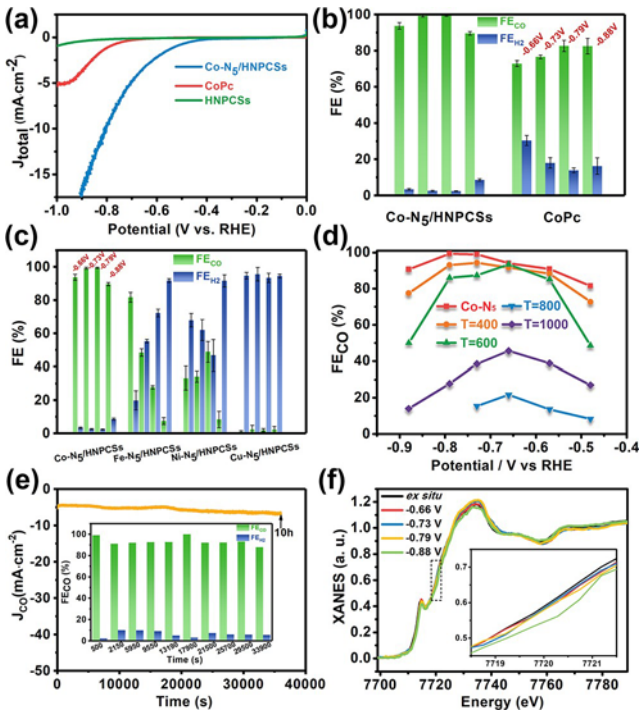

Figure 3. (a) LSV curves. FE_{CO} and FE_{H2} of (b) Co−N_5/HNPCSs and CoPc, (c) M-N_5/HNPCSs (M = Co, Fe, Ni, Cu) and (d) Co− N_5/HNPCSs-T. (e) Chronoamperograms at −0.73 V (inset is FE_{CO} and FE_{H2} at di□ erent time). (f) XANES of Co−N_5/HNPCSs catalyst under ex situ and in situ (inset is the magnified image).

In CO_2RR, different metal catalytic sites usually undergo different reaction pathways, which leads to the difference in FE. To probe the effect of metal sites on electrocatalytic activity, M−N_5/HNPCSs catalysts (M = Fe, Ni, Cu) are synthesized and characterized (Figures S6−S10, Tables S1 and S2). Interestingly, in terms of FE_{CO}, M−N_5/HNPCSs catalysts are found to be significantly inferior to Co−N_5/HNPCSs (Figure

3c), indicating the positive role of Co sites. To reveal the effect of coordination environment,the Co−N_5/HNPCSs catalyst was pyrolyzed at different temperature. Co−N_4/HNPCSs and Co−N_3/HNPCSs catalyst are obtained at 400 and 600°C, whereas higher temperature lead to the formation of NPs. (Figure 2b, Figures S11−S16, Tables S1 and S2). Figure 3d shows that the FE_{CO} (FE_{H2} shown in Figure S17) drops with the decrease of Co−N_x coordination. Electrocatalytic tests results indicate that the Co−N_5/HNPCSs has the highest FE_{CO} at −0.73 and −0.79 V vs RHE, and its FE_{CO} remains higher than 90% from −0.57 V to −0.88 V vs RHE. The Co−N_4/ HNPCSs and Co−N_3/HNPCSs exhibit relatively high CO_2 reduction ability at certain potentials, and the FE_{CO} of these two samples are around 90% from −0.57 to −0.79 V. Nevertheless, the formation of NPs results in the deactivation of catalyst in CO_2 electrolysis, namely, the FE_{CO} of Co−N_5/ HNPCSs-T (T = 800, 1000 °C) are lower than 50% at all potentials, indicating higher catalytic activity of single-atom site catalysts. Furthermore, the Co−N_5/HNPCSs also shows the highest turnover frequency (TOF) value (Figure S18a, 480.2 h^{-1}) and the largest CO partial current density (Figure S18b, ~4.5 $mA{\cdot}cm^{-2}$) at −0.73 V vs RHE among all the catalysts. The CO current density value and FE_{CO} remained nearly unchanged after electrolyzing 10 h at −0.73 V (Figure 3e), suggesting remarkable stability. The current density can be enhanced and the support morphology affect the charge transfer during electrolysis (Figures S19−S23).

In situ XAS results indicated that the Co K-edge XANES peaks are located at a higher energy than that of ex situ state in the reduction potential from −0.66 to −0.79 V, indicating that the valence state of Co becomes higher in electrolysis than ex situ state. However, when a higher potential (−0.88 V) is applied, the Co K-edge has a significant shift, whereas the FE_{CO} is decreased. These changes show that the appropriate electronic structure is important for CO_2RR (Figure 3f, Figure S24).

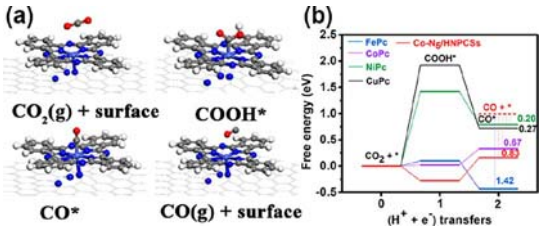

Figure 4. (a) Optimized structures for the intermediates. (b) Calculated free energy of CO_2RR (red short dash line, the desorption free energy level of CO; dash dot lines, the desorption free energy of CO).

DFT calculations are carried out to understand the intrinsic property and reactivity. The CO_2RR pathway is investigated via computational hydrogen electrode model[29] (Figure 4a). Therequired free energy change (ΔG) for CoPc from CO_2 to adsorbed COOH* is close to zero (0.02 eV), lower than that of NiPc (1.42 eV), CuPc (1.92 eV) and FePc (0.10 eV), indicating a higher CO_2RR activity (Figure 4b). The bond lengthchanges show the same sequence (Table S4). The ΔG from CO_2 to MPc_CO* are −0.43, 0.33, 0.79, 0.72 eV in the sequence of Fe, Co, Ni, Cu, and the CO desorption free energy level is 0.99 eV. The BE of CO on FePc and CoPc is −1.17 and −0.68 eV, suggesting CO tend to desorb on CoPc. The reaction may be blocked on the first proton-coupled electron-transfer step (PES) for NiPc (1.42 eV) and CuPc (1.92 eV). The free energy profile of CO_2RR on the Co−N_5/HNPCSs improves the ΔG of the first reduction step to −0.28 eV, and keep the CO* species progress close to CoPc. The improvement degree of ΔG for the first PES is 0.31 eV, whereas the increase of CO desorption free energy is 0.16 eV, thus making the effectivity of CO_2RR on Co−N_5/HNPCSs higher than on CoPc. Electron localization function (Figure S26) revealed that

the strong COOH interaction and moderate binding interaction of CO on Co center makes it ideal material for CO_2RR. In the context of chemisorption of COOH or CO, an approximately linear relationship is found between the adsorption energy E_{ads} and the d-band center E_{dbc}[30] (Figure S27 and Table S5).

In summary, we have developed an N-coordination strategy to atomically dispersed Co electrocatalyst with high selectivity in the conversion of CO_2 to CO. Significantly, the formed Co−N_5 site is found to be the active center for CO_2 activation and the rapid formation of key reaction intermediate COOH* as well as desorption of CO. This work not only designs a robust CO_2RR electrocatalyst but also provides an in-depth under- standing of the catalytic active centers.

ASSOCIATED CONTENT

Supporting Information

The Supporting Information is available free of charge on the ACS Publications website at DOI: 10.1021/jacs.8b00814.

Detailed experimental procedures; characterization meth- ods, and additional tables and figures (PDF)

AUTHOR INFORMATION

Corresponding Author

*cchen@mail.tsinghua.edu.cn

ORCID

Jun Li: 0000-0002-8456-3980

Dingsheng Wang: 0000-0003-0074-7633

Yadong Li: 0000-0003-1544-1127

Author Contributions

$^{\Delta}$Y.P., R.L. and Y.C. contributed equally.

Notes

The authors declare no competing financial interest.

ACKNOWLEDGMENTS

This work was supported by the National Natural Science Foundation of China (21573119, 21590792, 21521091, 21390393, U1463202, 91645203), China Ministry of Science and Technology under Contract of 2016YFA(0202801), China Postdoctoral Science Foundation (2017M610076), Beijing Natural Science Foundation (2184104) and the Fundamental Research Funds for the Central Universities (15CX06037A).

REFERENCES

(1) Schreier, M.; Heŕoguel, F.; Steier, L.; Ahmad, S.; Luterbacher, J.S.; Mayer, M. T.; Luo, J.; Grat□zel, M. Nat. Energy 2017, 2, 17087.

(2) Liu, C.; Colón, B. C.; Ziesack, M.; Silver, P. A.; Nocera, D. G.Science 2016, 352, 1210−1213.

(3) Larrazabal, G. O.; Martín, A. J.; Mitchell, S.; Hauert, R.; Perez- Ramírez, J. ACS Catal. 2016, 6, 6265−6274.

(4) Cao, Z.; Kim, D.; Hong, D.; Yu, Y.; Xu, J.; Lin, S.; Wen, X.; Nichols, E. M.; Jeong, K.; Reimer, J. A.; Yang, P.; Chang, C. J. J. Am. Chem. Soc. 2016, 138, 8120−8125.

(5) Kang, P.; Zhang, S.; Meyer, T. J.; Brookhart, M. Angew. Chem., Int. Ed. 2014, 53, 8709−8713.Sargent, E. H.; Klinkova, A.; Kumacheva, E. Nature 2016, 537, 382−386.

(6) Kumar, B.; Atla, V.; Brian, J. P.; Kumari, S.; Nguyen, T. Q.; Sunkara, M.; Spurgeon, J. M. Angew. Chem., Int. Ed. 2017, 56,

3645− 3649.

(7) Asadi, M.; Kim, K.; Liu, C.; Addepalli, A. V.; Abbasi, P.; Yasaei, P.; Phillips, P.; Behranginia, A.; Cerrato, J. M.; Haasch, R.; Zapol, P.; Kumar, B.; Klie, R. F.; Abiade, J.; Curtiss, L. A.; Salehi-Khojin, A. Science 2016, 353, 467.

(8) Schneider, J.; Jia, H.; Kobiro, K.; Cabelli, D. E.; Muckerman, J. T.; Fujita, E. Energy Environ. Sci. 2012, 5, 9502−9510.

(9) Liu, M.; Pang, Y.; Zhang, B.; De Luna, P.; Voznyy, O.; Xu, J.; Zheng, X.; Dinh, C. T.; Fan, F.; Cao, C.; Pelayo García de Arquer, F.; Safaei, T. S.; Mepham, A.; Filleter, T.; Sinton, D.; Kelley, S. O.;Sargent, E. H.; Klinkova, A.; Kumacheva, E. Nature 2016, 537, 382−386.

(10) Nie, X.; Esopi, M. R.; Janik, M. J.; Asthagiri, A. Angew. Chem., Int. Ed. 2013, 52, 2459−2462.

(11) Li, Q.; Fu, J.; Zhu, W.; Chen, Z.; Shen, B.; Wu, L.; Xi, Z.; Wang, T.; Lu, G.; Zhu, J. J.; Sun, S. J. Am. Chem. Soc. 2017, 139, 4290−4293.

(12) Kim, D.; Resasco, J.; Yu, Y.; Asiri, A. M.; Yang, P. Nat. Commun.2014, 5, 4948.

(13) Gao, S.; Lin, Y.; Jiao, X.; Sun, Y.; Luo, Q.; Zhang, W.; Li, D.; Yang, J.; Xie, Y. Nature 2016, 529, 68−72.

(14) Rao, H.; Schmidt, L. C.; Bonin, J.; Robert, M. Nature 2017, 548, 74−77.

(15) Lin, S.; Diercks, C. S.; Zhang, Y. B.; Kornienko, N.; Nichols, E.M.; Zhao, Y.; Paris, A. R.; Kim, D.; Yang, P.; Yaghi, O. M.; Chang, C. J.Science 2015, 349, 1208−1213.

(16) Zhang, X.; Wu, Z.; Zhang, X.; Li, L.; Li, Y.; Xu, H.; Li, X.; Yu, X.; Zhang, Z.; Liang, Y.; Wang, H. Nat. Commun. 2017, 8, 14675.

(17) Gao, D.; Zhang, Y.; Zhou, Z.; Cai, F.; Zhao, X.; Huang, W.; Li, Y.; Zhu, J.; Liu, P.; Yang, F.; Wang, G.; Bao, X. J. Am. Chem. Soc. 2017, 139, 5652−5655.

(18) Lu, Q.; Rosen, J.; Zhou, Y.; Hutchings, G. S.; Kimmel, Y. C.;Chen, J. G.; Jiao, F. Nat. Commun. 2014, 5, 3242.

(19) Huang, H.; Jia, H.; Liu, Z.; Gao, P.; Zhao, J.; Luo, Z.; Yang, J.; Zeng, J. Angew. Chem., Int. Ed. 2017, 56, 3594−3598.

(20) Liu, M.; Pang, Y.; Zhang, B.; De Luna, P.; Voznyy, O.; Xu, J.;Zheng, X.; Dinh, C. T.; Fan, F.; Cao, C.; Pelayo García de Arquer, F.; Safaei, T. S.; Mepham, A.; Klinkova, A.; Kumacheva, E.; Filleter, T.;Sinton, D.; Kelley, S. O.; Sargent, E. H. Nature 2016, 537, 382−386.

(21) Wu, Y.; Jiang, J.; Weng, Z.; Wang, M.; Broere, D. L. J.; Zhong, Y.; Brudvig, G. W.; Feng, Z.; Wang, H. ACS Cent. Sci. 2017, 3, 847− 852.

(22) Weng, Z.; Wu, Y.; Wang, M.; Jiang, J.; Yang, K.; Huo, S.; Wang, X. F.; Ma, Q.; Brudvig, G. W.; Batista, V. S.; Liang, Y.; Feng, Z.; Wang, H. Nat. Commun. 2018, 9, 415.

(23) Qiao, B.; Wang, A.; Yang, X.; Allard, L. F.; Jiang, Z.; Cui, Y.; Liu, J.; Li, J.; Zhang, T. Nat. Chem. 2011, 3, 634−641.

(24) Cao, Y.; Chen, S.; Luo, Q.; Yan, H.; Lin, Y.; Liu, W.; Cao, L.; Lu, J.; Yang, J.; Yao, T.; Wei, S. Angew. Chem., Int. Ed. 2017, 56, 12191− 12196.

(25) Zheng, Y.; Jiao, Y.; Zhu, Y.; Cai, Q.; Vasileff, A.; Li, L. H.; Han, Y.; Chen, Y.; Qiao, S. Z. J. Am. Chem. Soc. 2017, 139, 3336−3339.

(26) Jiang, K.; Siahrostami, S.; Akey, A. J.; Li, Y.; Lu, Z.; Lattimer, J.;Hu, Y.; Stokes, C.; Gangishetty, M.; Chen, G.; Zhou, Y.; Hill, W.; Cai,W. B.; Bell, D.; Chan, K.; Nørskov, J. K.; Cui, Y.; Wang, H. Chem.2017, 3, 950.

(27) Jiang, K.; Siahrostami, S.; Zheng, T.; Hu, Y.; Hwang, S.; Stavitski, E.; Peng, Y.; Dynes, J.; Gangisetty, M.; Su, D.; Attenkofer, K.; Wang, H. Energy Environ. Sci. 2018, DOI: 10.1039/C7EE03245E.

(28) Liu, J.; Qiao, S. Z.; Liu, H.; Chen, J.; Orpe, A.; Zhao, D.; Lu, G. Q. Angew. Chem., Int. Ed. 2011, 50, 5947−5951.

(29) Nørskov, J. K.; Rossmeisl, J.; Logadottir, A.; Lindqvist, L.; Kitchin, J. R.; Bligaard, T.; Jonsson, H. J. Phys. Chem. B 2004, 108, 17886−17892.

(30) Hammer, B.; Norskov, J. K. Nature 1995, 376, 238−240.